

Magnetic Structures Database from Symmetry-aided High-Throughput Calculations

Hanjing Zhou,^{1,2} Yuxuan Mu,^{1,2} Dingwen Zhang,^{1,2} Hangbing Chu,^{1,2} Di Wang,^{1,2} Huimei Liu,^{1,2} and Xiangang Wan^{1,2,3,4,*}

¹*National Laboratory of Solid State Microstructures and School of Physics, Nanjing University, Nanjing 210093, China*

²*Collaborative Innovation Center of Advanced Microstructures, Nanjing University, Nanjing 210093, China*

³*Hefei National Laboratory, Hefei 230088, China*

⁴*Jiangsu Physical Science Research Center, Nanjing University, Nanjing 210093, China*

(Dated: January 13, 2026)

Magnetic structures, which play a central role in determining their physical properties, are known for only very limited compounds. Traditional theoretical methods based on first-principles calculations are fundamentally limited by the need to calculate a large space of input magnetic configurations. Here we introduce a symmetry-aided strategy based on Landau's phase transition theory. By utilizing the crystallographic space group and the Wyckoff positions of magnetic ions, we narrow down the initial magnetic configurations to a limited number of candidates via the analysis of the group representations. The magnetic ground state is subsequently determined by the lowest energy of those well-selected magnetic configurations via first-principles calculations. Benchmarking calculations were performed on a subset of the MAGNCDATA database with wave vector $\mathbf{q} = 0$ and fewer than 40 atoms per unit cell, comprising 302 materials. Our method successfully identified the magnetic structures for 212 of these materials. We further apply our highly efficient method to 7,520 stoichiometric transition metal compounds with fewer than 20 atoms per unit cell in the Inorganic Crystal Structure Database, and establish a magnetic structure database containing 2,900 magnetic materials. To demonstrate the utility of our database, we apply it to the systematic exploration of magnetic topological phases and altermagnets, leading to the identification of 1,070 and 392 instances, respectively.

I. INTRODUCTION

Magnetic materials are pivotal to modern technology, enabling applications such as information storage, magnetic topology, spintronics and magnonics through their controllable magnetic response [1–8]. They also occupy a central position in condensed matter physics, providing a fertile platform for exploring fundamental collective phenomena that arise from electronic correlations, symmetry breaking, quantum fluctuations, etc. [9–14]. The defining characteristic of a magnetic material is its magnetic structure, the spatial arrangement of magnetic moments, which determines the magnetic space group and strongly influences its physical properties. Establishing the magnetic structure is therefore a prerequisite for studying magnetic phenomena.

Despite its importance, the determination of magnetic structures remains a major challenge. Experimentally, magnetic structures can be probed by techniques such as neutron diffraction, yet such methods are often facing technical constraints, including sample quality, crystal size, material-specific factors, and dimensionality [15, 16]. As a result, experimentally confirmed magnetic structures are available for only a small fraction of known magnetic compounds [17], underscoring the critical role of theoretical prediction.

While symmetry-based frameworks provide a rigorous and systematic language for describing magnetic config-

urations [18], theoretical prediction of magnetic ground states is most commonly carried out using first-principles total-energy calculations. A fundamental difficulty of such approaches is that they require initial magnetic configurations as input, which in principle have unlimited possibilities. Consequently, the central challenge lies in the absence of an efficient strategy to reduce the vast configuration space to a finite and physically relevant set of candidate magnetic states suitable for first-principles evaluation.

Important progress has been made along this line through a variety of strategies [19–24], including constrained searches focusing on collinear magnetism [21], stochastic optimization schemes such as genetic algorithms that explore magnetic configurations without explicit symmetry assumptions [22], the linear spin wave theory (LSWT)-based iterative optimization approach [23], and spin-spiral techniques that efficiently capture long-wavelength noncollinear magnetic orderings within simple magnetic unit cells and have successfully determined 194 magnetic structures [24]. In addition, Huebsch *et al.* [19, 20] employed a cluster multipole framework and applied it to the AtomWork-Adv database [25], which contains 228 magnetic compounds. However, magnetic materials exhibit a remarkable diversity of magnetic orderings, including both collinear and noncollinear states. Moreover, the Inorganic Crystal Structure Database (ICSD) [26] contains on the order of 10^5 materials hosting magnetic ions. These call for a scalable and highly efficient framework capable of treating the full diversity of magnetic orderings, including both collinear and noncollinear states, on an equal footing, irrespective

*The corresponding author: xgwan@nju.edu.cn.

of unit cell complexity.

Within the framework of Landau phase transition theory, we systematically narrow down the vast number of possible initial magnetic configurations to a finite set of candidates based on the irreducible representations (irreps) approach. First-principles total-energy calculations are then employed to identify the energetically favored ground state among these candidate magnetic orders. Benchmark calculations on 302 magnetic structures from MAGNDATA [17] show an agreement of about 70%. Applying this approach to compounds with propagation vector $\mathbf{q} = 0$ and fewer than 20 atoms per unit cell in ICSD [26], we construct a database comprising over 2,900 magnetic materials. As the magnetic structure fundamentally governs all the physical properties of a material, our magnetic structure database provides a broader materials basis for systematic investigations of physical properties, such as spintronics, magnonics, magnetic topology, multiferroics etc. [1–14]. As an illustration of its capabilities, we present its application to the systematic identification of magnetic topological phases and altermagnets.

II. METHOD

It is well known that most magnetic phase transitions are continuous and can be described within Landau's theory[27]. At the critical temperature, the order parameter emerges continuously from zero, and the resulting magnetic order can be characterized by the irreducible representation of the parent crystallographic space group. This motivates us to construct a set of symmetry-guided magnetic-structure candidates corresponding its irreducible representation. Our approach is as follows.

For a crystal containing N magnetic ions in the unit cell, magnetic configurations with propagation vector $\mathbf{q} = 0$ are described by the $3N$ components of the local magnetic moments, $\boldsymbol{\mu} = (m_{1x}, m_{1y}, m_{1z}, \dots, m_{Nx}, m_{Ny}, m_{Nz})$, where m_{na} denotes the magnetic-moment component of atom n along the crystallographic axis a . The $3N$ components of $\boldsymbol{\mu}$ provide a basis for representation Γ_{mag} , which is generally reducible and can be decomposed into irreducible representations as

$$\Gamma_{\text{mag}} = \sum_{\oplus i} n_i \Gamma_i^{(j)}. \quad (1)$$

Here, $\Gamma_i^{(j)}$ denotes an irreducible representation of dimension j from the parent crystallographic space group, and n_i is its multiplicity. The completeness relation $\sum_i n_i \cdot j = 3N$ ensures that all magnetic degrees of freedom are fully accounted for in this decomposition.

For a continuous phase transition, the magnetic space groups (MSGs) of the ordered phase must be a subgroup of the parent crystallographic space group. Taking into account the Wyckoff positions of the magnetic atoms,

we obtain a specific set of irreducible representations in Eq. (1), thereby reducing the space of candidate MSGs to those compatible with the corresponding instability channels. Namely, a continuous magnetic transition is driven by the instability of a single irreducible representation $\Gamma_i^{(j)}$ in Eq. (1), so that only the MSGs associated the irreducible representations appear in Eq. (1) need to be considered. Even after both the unstable irrep and its corresponding MSGs are fixed, the magnetic structure is, in general, still not uniquely determined. To construct explicit magnetic configurations, we therefore employ symmetry-adapted basis vectors of the irreducible representation. However, residual degrees of freedom remain even within this basis-vector description. In the following, we discuss the two distinct sources of this intrinsic non-uniqueness and describe how the associated degrees of freedom can be systematically constrained.

For multi-dimensional irreducible representations $\Gamma_i^{(j)}$ with $j > 1$, different linear combinations of the basis vectors are symmetry-allowed and may correspond to different MSGs. Although, in principle, the physically realized order parameter could be obtained by minimizing higher-order terms of the Landau free energy, this route is not adopted in the present work. Instead, we employ a symmetry-based criterion and retain, among the magnetic subgroups compatible with the irreducible representations, the one that preserves the highest possible symmetry[28, 29].

A second source of non-uniqueness arises when a given irreducible representation appears multiple times in the magnetic representation, i.e., $n_i > 1$ in Eq. (1). In this case, the magnetic structure depends on the particular choice of basis, since multiple symmetry-equivalent basis sets of the basis vectors exist. To eliminate this freedom and construct a finite set of physically realizable configurations, we generate magnetic structures by aligning magnetic moments along all high-symmetry crystallographic directions compatible with the MSGs.

For each candidate material, a finite set of symmetry-allowed magnetic structures associated with the relevant irreducible representations was generated using the procedure described above, thereby drastically reducing the magnetic configuration space to a finite number of initial states for first-principles calculations. First-principles total-energy calculations were then performed among these well-selected structures using the Vienna Ab initio Simulation Package (VASP) [30, 31], employing a spin-polarized GGA + SOC + U approach. The Coulomb interaction parameters U and J were taken as the averaged values recommended for transition-metal elements based on the linear-response scheme [32]. The ground-state magnetic structure was identified as the configuration with the lowest total energy. To illustrate our approach, the complete workflow with the noncollinear magnet Mn₃GaN [33] is presented in the Supplementary Materials [34]. This material is chosen as an example because it exhibits both sources of non-uniqueness discussed above.

We benchmark our framework against established magnetic structures compiled in the MAGNDATA database [17]. After excluding entries with fractional site occupancies, we restrict our analysis to systems with fewer than 40 atoms in the primitive unit cell and exclude lanthanoids and actinoids due to the challenges in accurately described within standard density functional theory [35]. To limit the computational cost at this stage, we focus on magnetic structures with a propagation vector $\mathbf{q} = 0$, and this leaves 328 materials for further consideration. After excluding 26 materials whose experimentally reported magnetic structures are incompatible with Landau-type continuous phase transitions (see Supplementary Materials [34]), we are left with 302 materials to be validated. By subjecting these materials to our framework, we successfully identify the experimentally reported magnetic ground states of 212 cases, corresponding to an overall accuracy of approximately 70%. Additional details can be found in the Outlook section and the Supplementary Materials [34].

Given that the benchmark yielded excellent results, we applied our framework to the Inorganic Crystal Structure Database (ICSD) [26]. Restricting to systems with unit cells containing fewer than 20 atoms and excluding lanthanoids and actinoids, we focused on $\mathbf{q} = 0$ structures and performed systematic high-throughput first-principles calculations to determine the magnetic ground states of 7,520 transition-metal compounds. Within this well-defined scope, our workflow identified 4,619 materials as non-magnetic. The remaining 2,901 magnetic materials were compiled into a magnetic structure database. The magnetic ground states, corresponding magCIF files, and associated information of these magnetic materials have been archived in the Supplementary Materials [34] and a searchable database, available at <https://magdatabase.nju.edu.cn>.

This database captures a broad diversity of magnetic configurations. Among the identified ground states, 2663 are collinear and 238 are noncollinear. From the viewpoint of magnetic classification, 1,444 materials exhibit ferromagnetic (FM) ordering, and 336 materials are classified as ferrimagnetic (FiM). 1,121 compounds exhibit antiferromagnetic (AFM) order with vanishing net magnetization, including 392 altermagnets. The classification statistics of the magnetic structures are shown in Fig. 1. A complete list of the magnetic materials classification statistics is presented in the Supplementary Materials [34].

Beyond serving as a catalog of magnetic ground states, we further apply the database to perform topological classification and altermagnets, as will be demonstrated below.

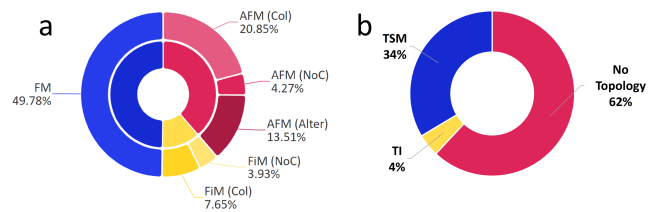


FIG. 1: **Magnetic and topological classification of our magnetic structure database.** (a) **Magnetic ground-state classification.** Among the 2,901 identified magnetic materials, 49.78% exhibit ferromagnetic (FM) ordering, 11.58% are ferrimagnetic (FiM), and the remaining 38.64% are antiferromagnetic (AFM). The FiM materials are further classified into 7.65% collinear (Col) and 3.93% noncollinear (NoC) states according to the relative orientation of magnetic moments. Within the AFM materials, 20.85% exhibit collinear (Col) order, 4.27% exhibit noncollinear (NoC) order, and 13.51% are classified as altermagnets (Alter). (b) **Topological classification of magnetic materials.** In total, 38% of the magnetic materials in the database are identified as magnetic topological materials, including 4% magnetic topological insulators (TIs) and 34% magnetic topological semimetals (TSMs).

III. MAGNETIC TOPOLOGICAL MATERIALS

For decades, the topology of electronic bands in condensed-matter materials has been a research hotspot [36], leading to a systematic classification of several tens of thousands non-magnetic topological materials based on the symmetry analysis [37–39]. Owing to the limited number of known magnetic structures [17], theoretical predictions of magnetic topological materials remain relatively scarce, with only a few hundred reported to date [3, 40]. Based on our magnetic structure database, we identify 1070 compounds as magnetic topological materials using magnetic topological quantum chemistry [41, 42]. They can be broadly classified into 125 magnetic topological insulators and 945 magnetic topological semimetals, as summarized in Fig. 1b. A complete list of materials and symmetry indicators is provided in the Supplementary Materials [34]. To illustrate the physical richness enabled by the symmetry-resolved magnetic structures, we select several representative materials shown below. We also tested the effects of varying the Hubbard U within reasonable ranges, and found that both their magnetic structures and topological properties remain unchanged.

A. Magnetic topological insulators

AFM axion insulator FeSe: The FeSe compound (icsd_166445) studied here crystallizes in the orthorhombic space group *Pnma* (No. 62) [43], which is different from the widely studied superconducting α -FeSe of the tetragonal structure *P4/nmm* (No. 129) [44, 45]. Our

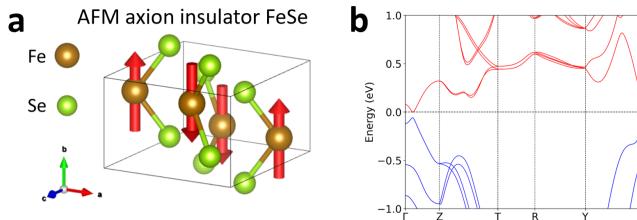


FIG. 2: AFM axion insulator FeSe. (a) magnetic structure (b) band structure. The green and yellow balls are Se and Fe ions, respectively. The magnetic moments of Fe are along the *b*-axis ([010]), as indicated by red arrow.

calculations predict an antiferromagnetic ground state in FeSe. It belongs to the magnetic space group *Pnma* (62.441), with magnetic moments oriented along the [010] direction, as shown in Fig. 2a. Due to the presence of inversion symmetry, symmetry indicators (η_{4I} , $z_{2I,1}$, $z_{2I,2}$, $z_{2I,3}$) can be defined using the parities at high-symmetry points [42]. η_{4I} is defined as the total number of odd-parity states at the eight time-reversal-invariant momenta (TRIMs) modulo 4, while $z_{2I,i}$ is defined as the total number of odd-parity states at the four TRIMs on the $k_i = \pi$ plane modulo 2. Our calculated symmetry indicators (η_{4I} , $z_{2I,1}$, $z_{2I,2}$, $z_{2I,3}$) are (2000). Furthermore, we find that all plane Chern numbers on the TRIM planes vanish for FeSe, and the system exhibits a direct band gap no smaller than 20 meV throughout the entire Brillouin zone, see Fig. 2b. The nontrivial symmetry indicators, together with a direct band gap throughout the entire Brillouin zone, indicate that FeSe is an axion insulator, in which a topological magnetoelectric effect is expected to occur [46, 47].

B. Magnetic topological semimetals

Noncollinear AFM Weyl semimetal V_3Ga_2 : The paramagnetic phase of V_3Ga_2 (icsd_635637) crystallizes in the space group *R32* (No. 155). The magnetic ground state of V_3Ga_2 is a noncollinear antiferromagnetic configuration, as shown in Fig. 3a, which belongs to the magnetic space group *R32* (155.45). The calculated band structure of V_3Ga_2 , shown in Fig. 3b, shows a Weyl point protected by the C_{2x} symmetry along the high-symmetry line Γ - F , as well as two Weyl points protected by the C_{3z} symmetry along the high-symmetry line T - Γ . A total of 28 Weyl points exist throughout the entire Brillouin zone, with their distribution shown in Fig. 3c, and their energies lying in the range from -7 to 28 meV.

AFM Dirac semimetal MnTe: The paramagnetic phase of MnTe (icsd_076241) has the space group *Pnma* (No. 62), which is the high-pressure structure of altermagnet α -MnTe [48, 49]. Under high pressure, α -MnTe undergoes a structural phase transition from the NiAs-type structure to the MnP-type structure [50]. We find that the magnetic ground state of MnTe (icsd_076241) is

a *PT* antiferromagnet, belonging to the magnetic space group *Pn'm'a'* (62.449), as shown in Fig. 3d. Throughout the entire Brillouin zone, two Dirac points are located on the high-symmetry line $k_y = 0$, $k_z = \pi$, while four Dirac points reside on the high-symmetry line $k_y = \pi$, $k_z = 0$, as shown in Fig. 3e and f.

FM nodal-line semimetal Co_3SnC : The Co_3SnC (icsd_108129) adopts an anti-perovskite structure with the *Pm $\bar{3}m$* (No. 221) space group [51]. Its magnetic ground state is a ferromagnet with magnetization oriented along the [001] direction. The magnetic structure and the calculated electronic band structure of Co_3SnC are shown in Fig. 3g and 3h. As shown in the Fig. 3i, two nodal rings appear on the high-symmetry planes $k_z = 0$ and $k_z = \pi$. The two crossing bands carry $+i$ and $-i$ eigenvalues of the mirror symmetry m_z , respectively, and are thus protected by m_z symmetry. In addition, 16 symmetry-unprotected Weyl points are present in the Brillouin zone, with energies ranging from -0.1 to 0.15 eV.

IV. ALTERMAGNETS

Altermagnets represent a recently identified magnetic class distinct from conventional antiferromagnets, garnering significant attention due to their unique electronic band structures and chiral magnon splitting [12, 13, 52].

In our database, we have identified 392 altermagnetic materials, many of which exhibit pronounced electronic spin splitting and chiral magnon splitting, with a complete list provided in the Supplementary Materials [34]. Here we highlight a representative example, CsV_2S_2O .

CsV_2S_2O crystallizes in space group No. 123, and its magnetic moments are aligned along [001] direction, see Fig. 4(a). It exhibits strong altermagnetic spin splitting along high-symmetry paths [Fig. 4(b)], reaching a maximum of approximately 1.7 eV near the X point, indicative of a pronounced electronic altermagnetic effect. The magnon spectrum shows a chiral splitting of up to 94.4 meV at the X point in the Brillouin zone, originating from two symmetry-inequivalent next-nearest-neighbor exchange interactions [34], in contrast to the typical origin which arises from disparities in long-range exchange interactions (e.g., J_{7a} versus J_{7b} in MnF_2 [53]). This value significantly exceeds the experimentally reported chiral magnon splittings in MnF_2 [53] and $MnTe$ [54].

V. OUTLOOK

We have developed a highly efficient methodology that addresses a bottleneck in magnetic materials research by combining symmetry analysis with first-principles calculations. For continuous magnetic phase transitions, the symmetry of the ordered phase follows a subgroup relation with respect to the parent space group. Using the Wyckoff positions of magnetic atoms, we construct the

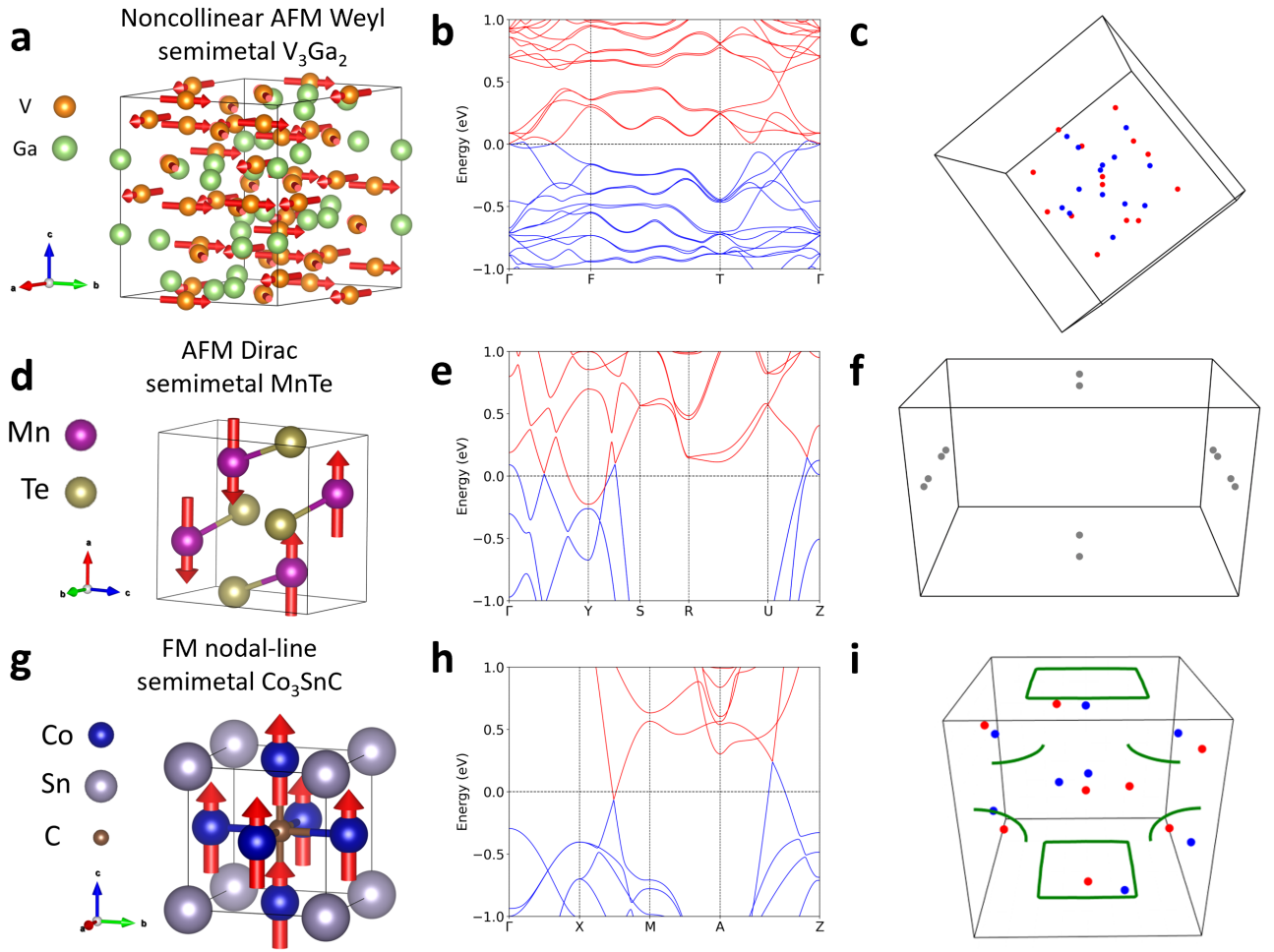


FIG. 3: Topological magnetic semimetals. (a)-(c) Magnetic structure, band structure, and distribution of Weyl points of the non-collinear AFM Weyl semimetal V_3Ga_2 . The magnetic moments of V lie in the xy plane, as indicated by red arrow. (d)-(f) Magnetic structure, band structure, and distribution of Dirac points of the AFM Dirac semimetal $MnTe$. (g)-(i) Magnetic structure, band structure, and distribution of nodal rings and Weyl points of the FM nodal-line semimetal Co_3SnC . The red and blue dots in (c) and (k) denote Weyl points with topological charges +1 and -1, respectively, while the green lines represent the nodal rings.

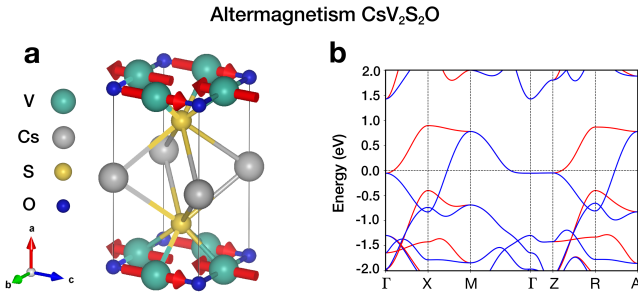


FIG. 4: (a) Crystal structure and (b) band structure of CsV_2S_2O .

magnetic representation and decompose it into the ir-

reducible representations of the parent crystallographic space group, thereby reducing the space of candidate MSGs to those compatible with the corresponding irreducible representations in Eq. (1). As the irreps and the corresponding MSGs do not uniquely fix the magnetic structure, we employ the symmetry-adapted basis vectors of the irreducible representation, which provide a more proper strategy for constructing explicit magnetic configurations, yet residual degrees of freedom remain. We further resolve these ambiguities by applying the maximal-symmetry criterion, and by aligning magnetic moments along all the highest-symmetry crystallographic directions. In this way, our approach yields a group theory based framework that drastically reduces the initial input magnetic configuration space and thereby enables efficient high-throughput first-principles calculations.

To empirically assess the validity of our developed symmetry-adapted approach, we analyzed the MAGN-DATA database for materials with $\mathbf{q} = 0$ and fewer than 40 atoms per primitive cell. Among the 328 materials examined, only 26 out of 328 are incompatible with Landau theory. For the remaining materials, deviations of magnetic moments from high-symmetry directions are found in only 23 out of 302 cases. These results show that the assumptions underlying our symmetry-based framework of using maximal symmetry criterion and aligning basis vector of irrep along all the highest-symmetry directions apply to the vast majority of known magnetic materials (i.e. 92%). When combined with first-principles calculations, the benchmark achieves an accuracy of about 70% (212 out of 302), with the remaining discrepancies mainly due to limitations of first-principles energetics. The applicability of our method is well justified by benchmarking tests.

The efficiency of our framework has enabled the construction of a comprehensive database of magnetic structures with $\mathbf{q} = 0$ and fewer than 20 atoms per primitive cell. Both constraints can be straightforwardly relaxed to incorporate commensurate propagation vectors and more atoms in unit cell. Extending the approach to two-dimensional magnetic materials is both natural and highly relevant, given the rapidly growing interest in low-dimensional magnetism. Beyond the topological

classification already accomplished, we are actively computing additional physical properties—including multiferroic responses, anomalous Hall conductivity, transport coefficients, etc.—for the magnetic materials identified in this work. These extensions are currently underway.

VI. ACKNOWLEDGEMENTS

This work was financially supported by the National Natural Science Foundation of China (Grants No. 12188101, No. 12574066, No. 12474233, and No. 12334007), the National Key R&D Program of China (Grant No. 2025YFA1411301, No. 2022YFA1403601), Innovation Program for Quantum Science and Technology (Grant No. 2021ZD0301902), Quantum Science and Technology-National Science and Technology Major Project (No. 2024ZD0300101), Natural Science Foundation of Jiangsu Province (No. BK20233001, BK20243011), Fundamental and Interdisciplinary Disciplines Breakthrough Plan of the Ministry of Education of China (JYB2025XDXM411), the Fundamental Research Funds for the Central Universities (No. KG202501). This work has been supported by the New Cornerstone Science Foundation.

[1] E. Dagotto, T. Hotta, and A. Moreo, “Colossal magnetoresistant materials: The key role of phase separation,” *PHYSICS REPORTS* **344**, 1 (2001).

[2] J. Coey, “Perspective and Prospects for Rare Earth Permanent Magnets,” *Engineering* **6**, 119 (2020).

[3] B. A. Bernevig, C. Felser, and H. Beidenkopf, “Progress and prospects in magnetic topological materials,” *Nature* **603**, 41 (2022).

[4] W. Eerenstein, N. D. Mathur, and J. F. Scott, “Multiferroic and magnetoelectric materials,” *Nature* **442**, 759 (2006).

[5] I. Žutić, J. Fabian, and S. Das Sarma, “Spintronics: Fundamentals and applications,” *Rev. Mod. Phys.* **76**, 323 (2004).

[6] W. Han, S. Maekawa, and X.-C. Xie, “Spin current as a probe of quantum materials,” *NATURE MATERIALS* **19**, 139 (2020).

[7] A. Chumak, V. I. Vasyuchka, A. A. Serga, and B. Hillebrands, “Magnon spintronics,” *Nature Physics* **11**, 453 (2015).

[8] P. A. McClarty, “Topological Magnons: A Review,” *Annual Review of Condensed Matter Physics* **13**, 171 (2022).

[9] C. Broholm, R. J. Cava, S. A. Kivelson, D. G. Nocera, M. R. Norman, and T. Senthil, “Quantum spin liquids,” *Science* **367**, eaay0668 (2020).

[10] M. Vojta, “Frustration and quantum criticality,” *Reports on Progress in Physics* **81**, 064501 (2018).

[11] H. v. Löhneysen, A. Rosch, M. Vojta, and P. Wölfle, “Fermi-liquid instabilities at magnetic quantum phase transitions,” *Rev. Mod. Phys.* **79**, 1015 (2007).

[12] L. Šmejkal, J. Sinova, and T. Jungwirth, “Emerging Research Landscape of Altermagnetism,” *Phys. Rev. X* **12**, 040501 (2022).

[13] L. Šmejkal, J. Sinova, and T. Jungwirth, “Beyond Conventional Ferromagnetism and Antiferromagnetism: A Phase with Nonrelativistic Spin and Crystal Rotation Symmetry,” *Phys. Rev. X* **12**, 031042 (2022).

[14] H.-Y. Ma, M. Hu, N. Li, J. Liu, W. Yao, J.-F. Jia, and J. Liu, “Multifunctional antiferromagnetic materials with giant piezomagnetism and noncollinear spin current,” *Nature Communications* **12**, 2846 (2021).

[15] V. Naish, R. P. Ozerov, and Y. A. Izyumov, *Neutron diffraction of magnetic materials* (Springer Science & Business Media, 2012).

[16] T. Yankova, D. Hüvonen, S. Mühlbauer, D. Schmidiger, E. Wulf, S. Zhao, A. Zheludev, T. Hong, V. Garlea, R. Custelcean, and G. Ehlers, “Crystals for neutron scattering studies of quantum magnetism,” *Philosophical Magazine* **92**, 2629 (2012).

[17] S. V. Gallego, J. M. Perez-Mato, L. Elcoro, E. S. Taschi, R. M. Hanson, K. Momma, M. I. Aroyo, and G. Madariaga, “MAGN-DATA: towards a database of magnetic structures. I. The commensurate case,” *Journal of Applied Crystallography* **49**, 1750 (2016).

[18] J. M. Perez-Mato, B. J. Campbell, V. O. Garlea, F. Damay, G. Aurelio, M. Avdeev, M. T. Fernández-Díaz, M. S. Henriques, D. Khalyavin, S. Lee, V. Pomjakushin, N. Terada, O. Zaharko, J. Campo, O. Fabelo, D. B. Litvin, V. Petricek, S. Rayaprol, J. Rodriguez-Carvajal, and R. Von Dreele, “Guidelines for commu-

nicipating commensurate magnetic structures. A report of the International Union of Crystallography Commission on Magnetic Structures," *Acta Crystallographica Section B* **80**, 219 (2024).

[19] M.-T. Huebsch, T. Nomoto, M.-T. Suzuki, and R. Arita, "Benchmark for Ab Initio Prediction of Magnetic Structures Based on Cluster-Multipole Theory," *Phys. Rev. X* **11**, 011031 (2021).

[20] T. Nomoto, S. Minami, Y. Yanagi, M.-T. Suzuki, T. Koretzune, and R. Arita, "High-throughput calculations of antiferromagnets hosting anomalous transport phenomena," *Phys. Rev. B* **109**, 094435 (2024).

[21] M. K. Horton, J. H. Montoya, M. Liu, and K. A. Persson, "High-throughput prediction of the ground-state collinear magnetic order of inorganic materials using Density Functional Theory," *npj Computational Materials* **5**, 64 (2019).

[22] F. Zheng and P. Zhang, "MagGene: A genetic evolution program for magnetic structure prediction," *Computer Physics Communications* **259**, 107659 (2021).

[23] A. Tellez-Mora, X. He, E. Bousquet, L. Wirtz, and A. H. Romero, "Systematic determination of a material's magnetic ground state from first principles," *npj Computational Materials* **10**, 20 (2024).

[24] J. Sødequist and T. Olsen, "Magnetic order in the computational 2D materials database (C2DB) from high throughput spin spiral calculations," *npj Computational Materials* **10**, 170 (2024).

[25] Y. Xu, M. Yamazaki, and P. Villars, "Inorganic Materials Database for Exploring the Nature of Material," *Japanese Journal of Applied Physics* **50**, 11RH02 (2011).

[26] D. Zagorac, H. Müller, S. Ruehl, J. Zagorac, and S. Rehme, "Recent developments in the Inorganic Crystal Structure Database: theoretical crystal structure data and related features," *Journal of Applied Crystallography* **52**, 918 (2019).

[27] A. Authier, *International tables for crystallography, volume D: Physical properties of crystals*, Vol. 4 (John Wiley & Sons, 2014).

[28] J. Perez-Mato, S. Gallego, E. Tasci, L. Elcoro, G. de la Flor, and M. Aroyo, "Symmetry-Based Computational Tools for Magnetic Crystallography," *Annual Review of Materials Research* **45**, 217 (2015).

[29] H. Zhou, S. Yan, D. Fan, D. Wang, and X. Wan, "Magnetic interactions and possible structural distortion in kagome fege from first-principles calculations and symmetry analysis," *Phys. Rev. B* **108**, 035138 (2023).

[30] G. Kresse and D. Joubert, "From ultrasoft pseudopotentials to the projector augmented-wave method," *Phys. Rev. B* **59**, 1758 (1999).

[31] G. Kresse and J. Furthmüller, "Efficient iterative schemes for ab initio total-energy calculations using a plane-wave basis set," *Phys. Rev. B* **54**, 11169 (1996).

[32] G. C. Moore, M. K. Horton, E. Linscott, A. M. Ganose, M. Siron, D. D. O'Regan, and K. A. Persson, "High-throughput determination of Hubbard U and Hund J values for transition metal oxides via the linear response formalism," *Phys. Rev. Mater.* **8**, 014409 (2024).

[33] D. Fruchart and E. F. Bertaut, "Magnetic studies of the metallic perovskite-type compounds of manganese," *Journal of the Physical Society of Japan* **44**, 781 (1978).

[34] See Supplementary Materials for "Magnetic Structures Database from Symmetry-aided High-Throughput Calculations".

[35] G. Kotliar, S. Y. Savrasov, K. Haule, V. S. Oudovenko, O. Parcollet, and C. Marianetti, "Electronic structure calculations with dynamical mean-field theory," *Reviews of Modern Physics* **78**, 865 (2006).

[36] M. Z. Hasan and C. L. Kane, "Colloquium: Topological insulators," *Rev. Mod. Phys.* **82**, 3045 (2010).

[37] T. Zhang, Y. Jiang, Z. Song, H. Huang, Y. He, Z. Fang, H. Weng, and C. Fang, "Catalogue of topological electronic materials," *Nature* **566**, 475 (2019).

[38] M. G. Vergniory, L. Elcoro, C. Felser, N. Regnault, B. A. Bernevig, and Z. Wang, "A complete catalogue of high-quality topological materials," *Nature* **566**, 480 (2019).

[39] F. Tang, H. C. Po, A. Vishwanath, and X. Wan, "Comprehensive search for topological materials using symmetry indicators," *Nature* **566**, 486 (2019).

[40] Y. Xu, L. Elcoro, Z.-D. Song, B. J. Wieder, M. G. Vergniory, N. Regnault, Y. Chen, C. Felser, and B. A. Bernevig, "High-throughput calculations of magnetic topological materials," *Nature* **586**, 702 (2020).

[41] J. Kruthoff, J. De Boer, J. Van Wezel, C. L. Kane, and R.-J. Slager, "Topological classification of crystalline insulators through band structure combinatorics," *Physical Review X* **7**, 041069 (2017).

[42] L. Elcoro, B. J. Wieder, Z. Song, Y. Xu, B. Bradlyn, and B. A. Bernevig, "Magnetic topological quantum chemistry," *Nature Communications* **12**, 5965 (2021).

[43] S. Margadonna, Y. Takabayashi, Y. Ohishi, Y. Mizuguchi, Y. Takano, T. Kagayama, T. Nakagawa, M. Takata, and K. Prassides, "Pressure evolution of the low-temperature crystal structure and bonding of the superconductor FeSe ($T_c = 37$ K)," *Phys. Rev. B* **80**, 064506 (2009).

[44] P. Zhang, K. Yaji, T. Hashimoto, Y. Ota, T. Kondo, K. Okazaki, Z. Wang, J. Wen, G. D. Gu, H. Ding, and S. Shin, "Observation of topological superconductivity on the surface of an iron-based superconductor," *Science* **360**, 182 (2018).

[45] D. Wang, L. Kong, P. Fan, H. Chen, S. Zhu, W. Liu, L. Cao, Y. Sun, S. Du, J. Schneeloch, R. Zhong, G. Gu, L. Fu, H. Ding, and H.-J. Gao, "Evidence for Majorana bound states in an iron-based superconductor," *Science* **362**, 333 (2018).

[46] X. Wan, A. M. Turner, A. Vishwanath, and S. Y. Savrasov, "Topological semimetal and fermi-arc surface states in the electronic structure of pyrochlore iridates," *Phys. Rev. B* **83**, 205101 (2011).

[47] X. Wan, A. Vishwanath, and S. Y. Savrasov, "Computational Design of Axion Insulators Based on 5d Spinel Compounds," *Phys. Rev. Lett.* **108**, 146601 (2012).

[48] J. Krempaský, L. Šmejkal, S. W. D'Souza, M. Hajlaoui, G. Springholz, K. Uhlířová, F. Alarab, P. C. Constantinou, V. Strocov, D. Usanov, W. R. Pudelko, R. González-Hernández, A. Birk Hellenes, Z. Jansa, H. Reichlová, Z. Šobáň, R. D. Gonzalez Betancourt, P. Wadley, J. Sinova, D. Kriegner, J. Minář, J. H. Dil, and T. Jungwirth, "Altermagnetic lifting of kramers spin degeneracy," *Nature* **626**, 517 (2024).

[49] S. Lee, S. Lee, S. Jung, J. Jung, D. Kim, Y. Lee, B. Seok, J. Kim, B. G. Park, L. Šmejkal, C.-J. Kang, and C. Kim, "Broken Kramers Degeneracy in Altermagnetic MnTe," *Phys. Rev. Lett.* **132**, 036702 (2024).

[50] M. Mimasaka, I. Sakamoto, K. Murata, Y. Fujii, and A. Onodera, "Pressure-induced phase transitions of MnTe," *J. Phys. C: Solid State Phys.* **20**, 4689 (1987).

- [51] S. Lin, P. Tong, B. Wang, J. Lin, Y. Huang, and Y. Sun, “Good Thermoelectric Performance in Strongly Correlated System SnCCo_3 with Antiperovskite Structure,” *Inorg. Chem.* **53**, 3709 (2014).
- [52] R. Xu, Y. Gao, and J. Liu, “Chemical design of monolayer altermagnets,” *National Science Review* , nwaf528 (2025).
- [53] V. C. Morano, Z. Maesen, S. E. Nikitin, J. Lass, D. G. Mazzone, and O. Zaharko, “Absence of Altermagnetic Magnon Band Splitting in MnF_2 ,” *Phys. Rev. Lett.* **134**, 226702 (2025).
- [54] Z. Liu, M. Ozeki, S. Asai, S. Itoh, and T. Masuda, “Chiral Split Magnon in Altermagnetic MnTe ,” *Phys. Rev. Lett.* **133**, 156702 (2024).